One-step bonding of Ni electrode to n-type PbTe - A step towards fabrication of thermoelectric generators

FERRERES, X.R., AMINORROAYA YAMINI, Sima <http://orcid.org/0000-0002-2312-8272>, NANCARROW, M. and ZHANG, C.

One-step bonding of Ni electrode to *n*-type PbTe – a step towards fabrication of thermoelectric generators

Xavier Reales Ferreres[1], Sima Aminorroaya Yamini[1*], Mitchell Nancarrow[2], Chao Zhang[1]

1. *Australian Institute for Innovative Materials (AIIM), Innovation Campus, University of Wollongong, Squire Way, North Wollongong , NSW 2500 , Australia*
2. *Electron Microscopy Centre (EMC), Innovation Campus, University of Wollongong, Squire Way, North Wollongong , NSW 2500 , Australia*

Corresponding author: *Sima Aminorroaya Yamini, email: sima@uow.edu.au*

Abstract

PbTe-based thermoelectric materials are good candidates for harvesting waste heat at mid-range temperatures due to their high thermoelectric efficiencies. Excellent quality and reliability of the bonding between the thermoelectric material and the electrode at high temperatures are essential for manufacturing thermoelectric generators. Here, a technique has been developed to achieve high-quality bonding between PbTe and the electrode. We have successfully performed one-step sintering of nickel electrode to *n*-type PbTe powder using spark plasma sintering. The fabricated interphase, composed of nickel telluride, is continuous and homogeneous across the junction, without visible flaws on the electrode or in the interphase and PbTe. To evaluate the long-term thermal stability of the fabricated bond, an aging test was conducted at 823 K for 360 hours under vacuum. The microstructures and chemical composition of the fabricated bonding and the aged sample were investigated in detail by scanning electron microscopy equipped with energy dispersive X-ray spectroscopy analysis. No excess reaction was observed between the electrode and the thermoelectric material after aging, supporting the formation of a chemically stable interphase, which acts as a diffusion barrier. Degradation of the PbTe was detected after aging, however. The fabricated interface meets the required criteria for maximum efficiency of PbTe materials.

Keywords

PbTe, Nickel, Thermoelectric module, One-step sintering, Interface

Introduction

Lead chalcogenides are known for their high thermoelectric performance in both *n*-type [1-3] and *p*-type [4-6] compounds at temperatures ranging from 500 K to 900 K. This makes them excellent choices as materials for solid-state thermoelectric generators designed for harvesting waste heat [7]. PbTe-based materials have been used in radioisotope thermoelectric generators (RTGs) [8] and more recently, in terrestrial applications [9] due to the latest improvements in their thermoelectric figure of

merit (zT). Nevertheless, a thermoelectric generator not only bases its performance efficiency on the high thermoelectric efficiency (zT) of its *p* and *n* couples, but also on good contacts with the electrodes [10]. Thermoelectric materials are joined to metal electrodes either through direct reaction [11] or by fabricating intermediate layers as diffusion barriers [12]. In either case, the obtained interphases are required to: (i) inhibit continuous reaction between the thermoelectric materials and the electrodes [13]; (ii) provide mechanical stability with no major defects or fractures [12]; (iii) have low thermal resistance [14]; and (iv) create ohmic contacts with low electrical resistance to eliminate voltage thresholds at the junction, which can diminish the total performance of the generator [15].

One of the major challenges is the choice of electrical contact (electrode), which should have minimum thermal mismatch with the thermoelectric material at the generator's working temperatures [16]. To maintain a reliable and lasting mechanical bond and to meet expectations of generator performance, comparable coefficients of thermal expansion (CTE) are essential for the thermoelectric material, the electrode, and any interphase that is formed [17]. Lead telluride is known for its high CTE, 20×10^{-6}/K, when compared to the metals (Ni, Fe) commonly used as electrodes. This makes it more difficult to bond PbTe to an electrode due to the stress caused by thermal expansion [18]. Nevertheless, Ni (CTE = 13.4×10^{-6}/K) and Fe (CTE = 11.8×10^{-6}/K) were studied as electrode materials for PbTe [11, 19]. The Fe/PbTe joint was found to be successful for *n*-type material, revealed as a mechanically stable joint with a low electrical resistance at the junction [19]. Temperatures as high as 1073 K were employed to form the Fe/PbTe joint [20], however, which might damage the PbTe. Nickel was joined to PbTe thermoelectric material by plasma activated sintering for the first time by Orihashi et al. [21], and the joint showed low electrical resistance at the contacts. Recently, in a study by Xia et al. [11], the same elements were bonded by a one-step hot press process, simultaneously consolidating and bonding the thermoelectric material to the electrode, and the detailed microstructures and composition of the interface were reported. It appears that Ni is a more viable electrode for PbTe than Fe.

Various approaches have been employed to create an effective diffusion barrier (interphase) between the thermoelectric material and the electrode, such as metallic thin film deposition [12, 22], soldering [23], brazing [24], and metallization processes [11, 25]. Recently, fabrication of bulk thermoelectric materials by the spark plasma sintering (SPS) technique has become more popular due to the fast sintering of high-quality dense products [26]. This technique has also been employed to bond electrodes to skutterudite [27, 28] or magnesium silicide based thermoelectric materials [25]. In this study, one-step bonding of *n*-type PbTe to high purity Ni plate was achieved by SPS. The chemical composition and microstructures at the interface were investigated in detail. We demonstrate a homogeneous interphase between the Ni electrode and the *n*-type PbTe. The thermal stability of the interphase and the thermoelectric material were also studied by aging the assembly at 823 K for 360 hours.

Materials and Methods

Polycrystalline $PbTe_{0.9988}I_{0.0012}$ was synthesized by mixing stoichiometric quantities of high purity Pb (99.999%), Te (99.999%), and PbI_2 in vacuum-sealed quartz ampoules and then heat-treating them at 1373 K for 10 hours. The samples were quenched in cold water, followed by annealing at 823 K for 72 hours. The obtained *n*-type lead telluride ingots were hand ground to a fine powder in a protective atmosphere. The powder (Figure 1(a)), consists of particles under 10 µm in size with a random distribution. The obtained powder was sintered into 12 mm diameter disk-shaped pellets using spark plasma sintering (SPS) at 793 K and axial pressure of 40 MPa for 30 minutes.

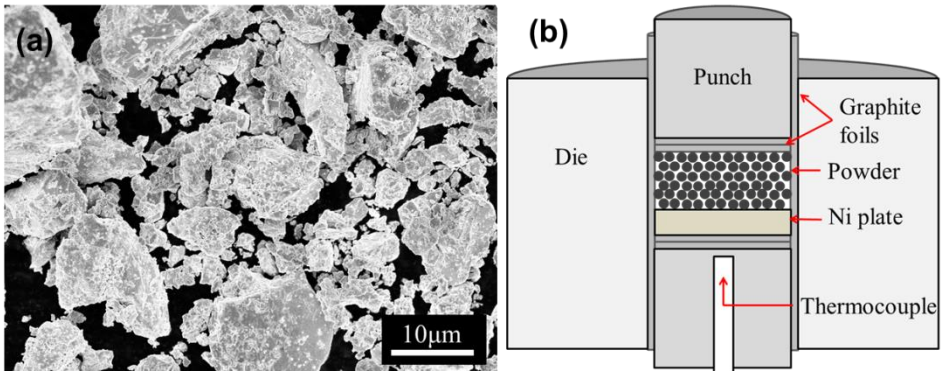

Figure 1. (a) SEM micrograph of hand-ground *n*-type PbTe fine powder, showing particles smaller than 10 µm; (b) schematic illustration of the experimental set-up in SPS.

The laser flash method (Linseis LFA 1000) was used to measure the thermal diffusivity (D_T). The thermal conductivity was calculated from $k = \rho D T c_p$, where the density (ρ) was calculated using the measured weight and dimensions. The specific heat capacity (c_p) was estimated by $c_p = 3.07 + 4.7\times10^{-4}\times(T[K] - 300)$. The electrical resistivity and Seebeck coefficient were measured using a Linseis LSR-3 instrument.

In order to sinter the PbTe powder to the Ni plate, a disk-shaped nickel plate with a thickness of 500 µm was polished to 1 µm surface roughness and ultrasonically cleaned with ethanol to remove possible contaminants on the surface. Subsequently, 1 g of PbTe powder was assembled with the Ni plate in a 12 mm graphite die. Figure 1(b) illustrates the layered structure of the assembly. The temperature was measured with a thermocouple located inside the bottom punch, close to the surface of the nickel plate. Graphite foil was used between the die, punches, and assembly to improve thermal contact and force distribution. The consolidation of the assembly was carried out by SPS at 773 K, 793 K, and 873 K, with uniaxial pressure of 40 MPa for 10 minutes under vacuum. Heating and cooling rates of 5 K/min were used.

The chemical composition and crystallographic structure of the reaction product between PbTe and Ni was characterized by X-ray diffraction (XRD) on a GBC MMA using Cu Kα radiation (λ = 1.544 Å,

40 kV, 25 mA). In order to investigate the microstructure and determine phases, the sample was prepared for electron back-scattering diffraction (EBSD) by manual grinding down to 12.3 μm, followed by cross-sectional ion milling on a Leica TIC-020.

EBSD and energy dispersive X-ray spectroscopy (EDS) information was obtained simultaneously from a 80×60 μm^2 area using a JEOL JSM-7001F field emission gun–scanning electron microscope (SEM) operating at 15 kV accelerating voltage, ~5.5 nA probe current, and 1500× magnification. The microscope was fitted with a Nordlys-II EBSD detector and an 80 mm^2 X-Max EDS detector interfacing with the Oxford Instruments Aztec software suite. The EBSD mapping conditions were optimised beforehand with 44, 42, and 40 reflectors employed for the Ni, Ni_3Te_2, and PbTe phases, respectively, as well as 4×4 binning, 2 background frames, a Hough resolution of 50, and concurrently indexed individual Kikuchi patterns up to 8 bands after preliminary EDS identification of the phases using TruPhase. The raw EBSD map returned an overall indexing rate of 98.65%, such that the zero solutions were concentrated at (sub)grain boundaries or phase interfaces. The map step size of 0.095 μm that was employed was equivalent to an EDS map resolution of ~2048×2048 pixels. Other EDS–based settings included a 20 keV energy range, auto-selection of the number of channels, a process time of 3 and a detector dead time of ~55–60%.

Thermoelectric modules for power generation are commonly encapsulated in inert atmosphere or under vacuum [8, 29]. In order to assess the thermal stability of the joints, PbTe/Ni samples were heat-treated at 823 K for 360 hours in a vacuum-sealed quartz tube. The microstructure analysis was also carried out for the heat-treated samples.

Results and Discussion

Figure 2(a) and (b) shows the thermoelectric transport properties of the fabricated *n*-type PbTe. These values are consistent with previous studies [1, 30] for *n*-type PbTe, indicating a thermoelectric figure of merit of roughly 1.2 at 700 K for a heavily doped compound.

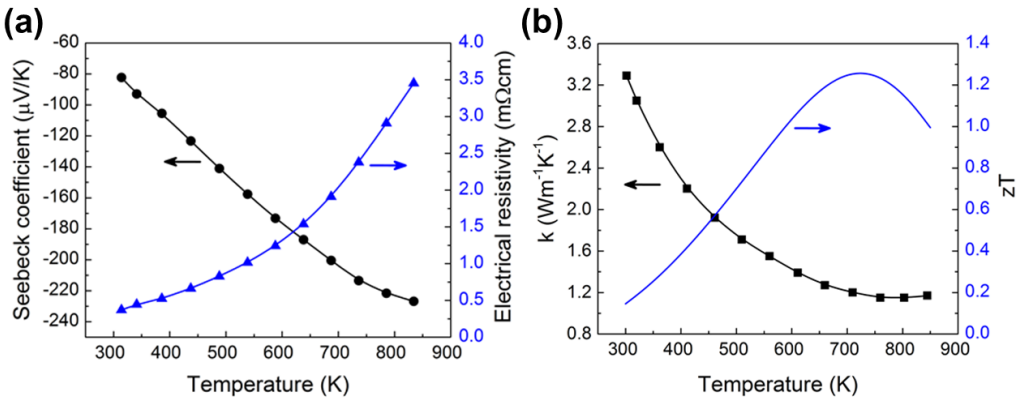

Figure 2. (a) Seebeck coefficient and electrical resistivity; (b) total thermal conductivity and figure of merit (*zT*) of $PbTe_{0.9988}I_{0.0012}$ as a function of temperature.

The back-scattered electron (BSE) micrograph in Figure 3(a) presents the entire cross section of the Ni plate and *n*-type PbTe interface, which were bonded at 793 K for 10 minutes. A continuous diffusion barrier layer is formed between the PbTe and the Ni along the roughly 10 mm length of the assembly. We can observe dense lead telluride without visible cracks, major porosity, or defects, as opposed to the interface with PbTe that was directly hot pressed to Ni [19], where cracks were observed in the nickel electrode.

Figure 3(b) and its inset show higher magnification micrographs of the bonding region, confirming the good cohesion between the PbTe, the interphase, and its Ni counterpart, with a homogeneous and smooth diffusion layer. The thickness of the interphase, shown in the inset of Figure 3(b), as measured from the SEM image, is approximately 27 μm. The EDS line scanning analysis, using SEM, in Figure 3(b) confirms an interphase thickness of around 27 μm, indicating the overall homogeneity of the reaction within the length of the sample. Figure 3(b) also demonstrates a clear compositional separation of layers. The interphase layer contains Ni and Te, whereas it is lead-free. No pure nickel was detected within the interphase layer, and the Ni content was reduced to zero in the PbTe layer.

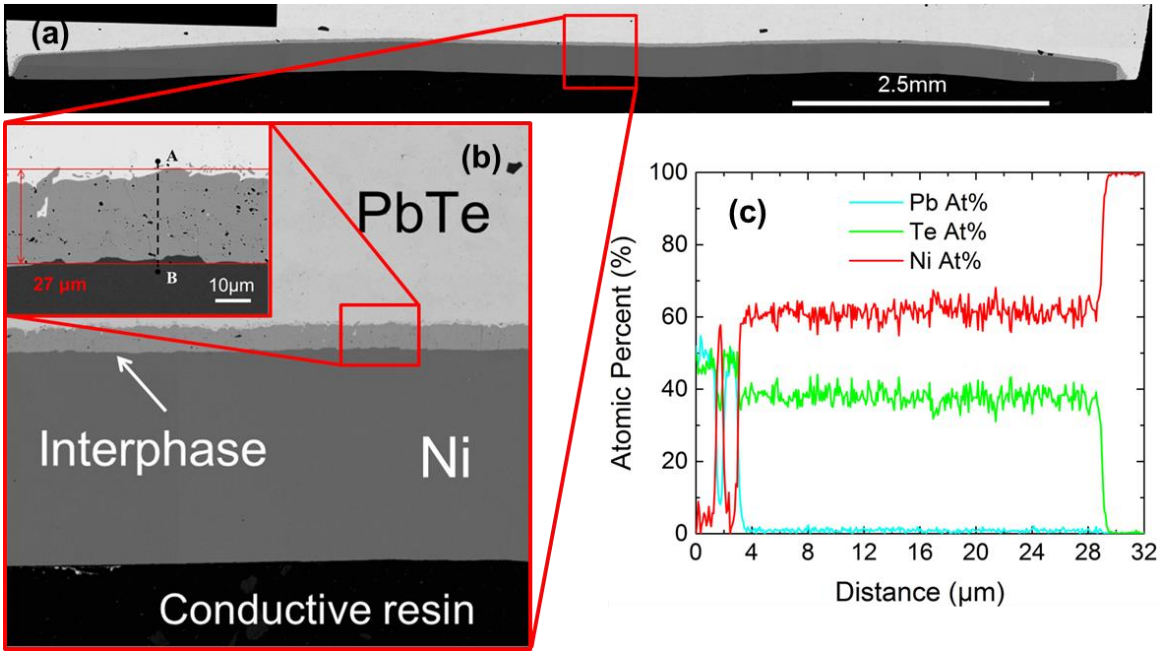

Figure 3. (a) SEM image of entire cross-section of PbTe powder sintered to Ni plate at 793 K using SPS; (b) SEM micrograph of indicated region in (a) with the inset showing higher magnification; and (c) line scan of AB line in inset image in (b).

In order to identify the crystallographic structure of the interphase formed between Ni and PbTe, the Ni plate was polished to a thickness of a few tens of micrometres, and the X-ray diffraction pattern was obtained from the surface of the sample (Figure 4). It is worth noting that due to manual polishing of the assembly, the PbTe phase was also exposed to the surface in some areas of the sample surface. The XRD pattern indicates the presence of three major phases. Ni and PbTe are identified with clear high intensity diffraction peaks, marked by red and yellow symbols in Figure 4. The higher intensity of the Ni peaks is due to the sample set-up on the X-ray diffraction equipment. The X-rays collided first with the Ni plate and then reached the interphase layer and PbTe. The low concentration of interphase layer resulted in peaks with lower intensities, which are identified as the β_2 $Ni_{3\pm x}Te_2$ phase. Slight variations in the composition of the β_2 $Ni_{3\pm x}Te_2$ phase occur as a function of temperature. Changes in the crystallographic structure from monoclinic to orthorhombic and then tetragonal occur at 491 K and 610 K, respectively [31]. The similarity of the lattice parameters of the three above-mentioned crystallographic structures [32] means that they cannot be distinguished in the obtained XRD diffraction pattern. Therefore, electron backscatter diffraction (EBSD) analysis was performed on the interphase to discern the β_2 phases.

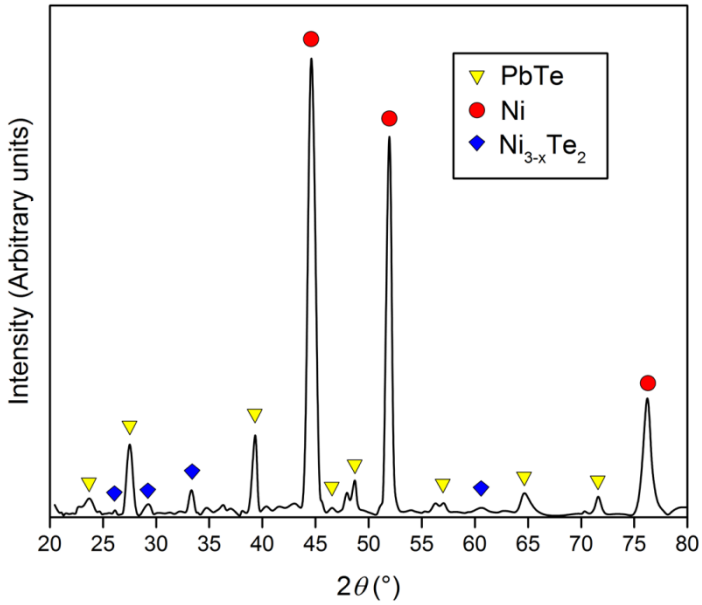

Figure 4. X-ray diffraction pattern of bonding area between PbTe and Ni, after sintering at 793 K under 40 MPa for 10 minutes, indicating Ni, PbTe, and $Ni_{3\pm x}Te_2$ phases.

Figure 5(a) and (b) depicts the EBSD band contrast and phase distribution maps, respectively. Figure 5(a) shows that the bottom layer comprises large Ni grains, whereas the middle and top layers comprise the Ni_3Te_2 phase, which has a monoclinic crystalline structure, and the PbTe phases, respectively. The indexing of the EBSD map was robust, such that the three phases are distinctly delineated using light red, blue, and yellow in Figure 5(b), respectively. With respect to the interphase layer of Ni_3Te_2 grains, it is of interest to note that they contain twins that have an 82.5°/<110> angle-axis relationship with the parent matrix. While a majority of the twin boundaries (shown in deep red in Figure 5(a) and (b)) are successfully identified, finer twins (whose boundaries show a darker band contrast than the parent matrix in Figure 5(a)) were not indexed due to the relatively coarse, 0.095 μm, step size used during mapping. A further observation is the prevalence of intergranular cracks between grains of the Ni_3Te_2 phase. These cracks and small pores were not indexed on the EBSD map and are shown in white in Figure 5(b). Simultaneous EDS elemental mapping was acquired during EBSD analysis. Figure 5(c), (d), and (e) show the distribution of Ni, Te, and Pb elements in the individual phases respectively. PbTe and Ni phases are distinct in chemical composition, and the interphase is rich in Ni and Te, and almost free of Pb. Table 1 presents the chemical compositions in atomic percentage of the layers of Ni, Ni_3Te_2, and PbTe analysed by EDS. These values were obtained by averaging several points and areas on the corresponding parts. The EDS quantitative analysis obtained from the interphase shows a Ni/Te atomic ratio of roughly 3:2, which agrees with the EBSD results.Therefore, we propose that the following reaction occurs during sintering of Ni to PbTe:

$$\boldsymbol{3Ni(s) + 2PbTe(s) \rightarrow Ni_3Te_2(s) + 2Pb(l)} \quad (1)$$

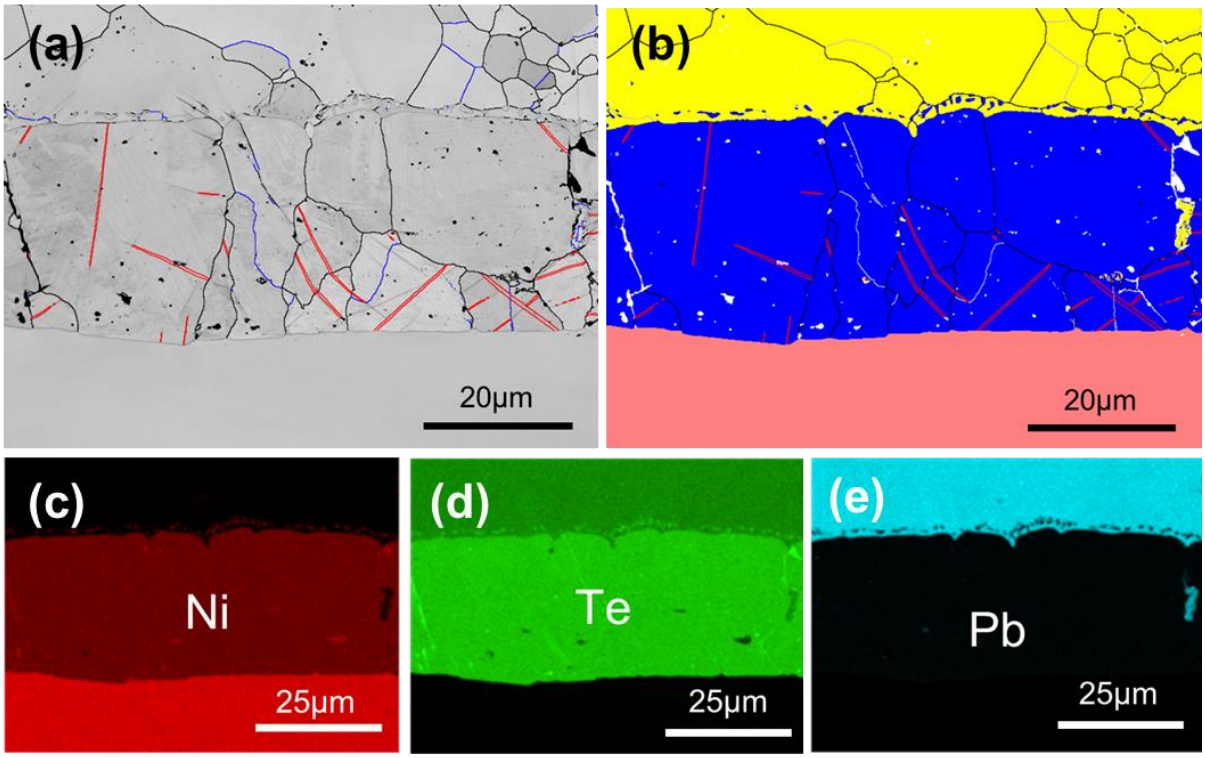

Figure 5. (a) EBSD band contrast map, (b) EBSD phase distribution map. EDS mapping of bonded PbTe/Ni at 793 K under 40 MPa for 10 minutes: (c) Ni elemental mapping, (d) Te elemental mapping, (e) Pb elemental mapping.

Table 1. Atomic percentage compositions given by EDS analysis on Figure 5(c), (d), and (e).

Areas	Ni (at. %)	Te (at. %)	Pb (at. %)
Ni	100	-	-
Ni_3Te_2	61.25	37.84	0.910
PbTe	-	49.45	50.55

The possibility of the formation of β_2 phase as a result of the reaction between Ni and PbTe at 793 K was studied thermodynamically. Table 2 lists the heat capacity (c_p) values as a function of temperature for the phases involved in the reaction. EBSD study confirmed that the thus-formed interphase is β_2 $Ni_{3\pm x}Te_2$ phase, so γ_1 phase ($Ni_{1.29}Te$, 43.7 at.% Te) and δ phase ($NiTe_{2-x}$, 52.2-66.7 at.%), which are also stable phases at room temperature [31, 32], are excluded from the thermodynamic calculations. Table 3 summarises the enthalpy, entropy, and Gibbs free energy of the components in Equation (1) at 793 K and at room temperature.

Table 2. Heat capacity (c_p) values of the phases involved in the chemical reaction during the sintering process as a function of temperature.

Phase label	Reference Formula	Temperature range (K)	$c_p(T[K])$ (J/mol K)	Ref.
β_2 ($Ni_{3\pm x}Te_2$, 38.8-41 at. % Te)	$Ni_{0.6}Te_{0.4}$	298.15 – 491.00	$\mathbf{18.018 + 8.003 \cdot 10^{-3}T + 2.651 \cdot 10^{-5}T^2 + 2.799 \cdot 10^{5}T^{-2}}$	[31]
		491.00 – 610.00	$\mathbf{118.871 - 0.184T + 1.121 \cdot 10^{-4}T^2 - 6.295 \cdot 10^{6}T^{-2}}$	
		610.00 – 793.15	$\mathbf{54.715 - 3.430 \cdot 10^{-2}T + 1.555 \cdot 10^{-5}T^2 - 3.006 \cdot 10^{6}T^{-2}}$	
PbTe	PbTe	298.15 – 793.15	$\mathbf{23.556 + 9.749 \cdot 10^{-3}T}$	[33]
Pb	Pb	298.15 – 601.00	$\mathbf{23.556 + 9.749 \cdot 10^{-3}T}$	[34]
		601.00 – 793.15	$\mathbf{32.426 - 3.096 \cdot 10^{-3}T}$	
Ni	Ni	298.15 – 793.15	$\mathbf{12.535 + 35.815 \cdot 10^{-3}T + 2.469 \cdot 10^{5}T^{-2}}$	[34]

Table 3. Thermodynamic data calculated from the c_p values in Table 2. Values of entropy (S_T), enthalpy (H_T), and Gibbs free energy (G_T) are calculated at room temperature and at 793 K.

Phase label	Used formula	Temperature (K)	S_T (J/Kmol)	H_T (kJ/mol)	G_T (kJ/mol)	Ref.
β_2 ($Ni_{3\pm x}Te_2$, 38.8-41 at. % Te)	Ni_3Te_2	298.15	200.00	-115.00	-174.63	[31]
		793.15	348.37	-39.015	-315.33	
PbTe	PbTe	298.15	110.04	-68.618	-101.43	[33]
		793.15	160.60	-43.255	-170.63	
Ni	Ni	298.15	29.874	0.0000	-8.9069	[34]
		793.15	60.024	15.576	-32.032	
Pb	Pb	298.15	64.785	0.0000	-19.316	[34]
		793.15	99.810	18.440	-60.724	

Table 4 summarises the entropy ($\Delta_r S_T$), enthalpy ($\Delta_r H_T$), and Gibbs free energy ($\Delta_r G_T$) of the reaction at room temperature and at 793 K. The $\Delta_r G_T$ of the reaction is slightly above zero and may suggest that the spontaneous reaction of compounds at 793 K is impossible. The temperature of the assembly in the SPS was measured at a distance from the area of the reaction, however, resulting in a few degrees difference between the actual temperature of the interface and the measured temperature. A previous study [35] suggested a reaction temperature of 793 K for β nickel telluride, when the thermodynamic data was adopted from different references to calculate the Gibbs free energy of the reaction.

Table 4. Thermodynamic data calculated for the reaction of PbTe with Ni.

Chemical reaction	Temperature (K)	$\Delta_r S_T$ (J/K mol)	$\Delta_r H_T$ (kJ/mol)	$\Delta_r G_T$ (kJ/mol)
$3Ni + 2PbTe \rightarrow Ni_3Te_2 + 2Pb$	298.15	19.868	22.236	16.312
	793.15	46.731	37.647	0.5827

According to both the pseudo-binary phase diagram of Ni-PbTe [36] and Equation (1), one of the reaction products of Ni with PbTe during sintering is pure lead, with a melting point of 600 K. Nevertheless, no pure Pb was observed by detailed microscopy of the cross-section of the sintered sample. Through stoichiometric calculations using Equation (1) and considering the densities of the different layers plus the volume of the die, we estimate that there should be a layer of Pb approximately 20 μm in thickness at the interface. Therefore, Pb, if it exists, should be easily identified in the SEM images. No trace of Pb was found in the sample during microscopy analysis, however. The melting point of Pb (600 K) is lower than the sintering temperature of 793 K. The observed small quantity of sintered material on the inner walls of the graphite die suggests an expulsion mechanism. We propose that the liquid Pb that was generated during the heating process was forced to leave the interface by the high uniaxial pressure. The expulsion of materials with lower melting points than the sintering temperature was previously reported during sintering by SPS [37].

In order to confirm the optimal bonding temperature for the PbTe/Ni, the interface of Ni with PbTe powder was studied after sintering at various temperatures under 40 MPa pressure for 10 minutes. Figure 6 shows the bonded areas for the 723 K, 793 K, and 873 K sintering temperatures. Figure 6(a) and (b) presents the backscattered electron (BSE) micrographs of the Ni and the *n*-type PbTe interface, which was bonded at 723 K. Ni plate was successfully bonded to well-sintered PbTe, and inhomogeneous reaction products were observed on the PbTe side near the PbTe/Ni interface. On the other hand, Figure 6(c) and (d) exhibits a homogeneous interphase for the reaction temperature of 793 K. The thickness of the interphase has also increased from ~3 μm to ~27 μm. When the sintering temperature was further increased to 873 K (Figure 6(e) and (f)), the thickness of the reaction layer (interphase) remained roughly constant. This could indicate a spontaneous reaction at a reaction temperature of ~793 K, forming a barrier layer, resulting in no further reaction between PbTe and Ni at higher temperatures. Nevertheless, small particles with the composition of the interphase in close proximity to the interface (PbTe/interphase) in Figure 6(d) have disappeared in Figure 6(f). These particles may have joined the interphase at higher sintering temperatures. More cracks and defects were observed in the sample sintered at 873 K. A continuous diffusion barrier layer is formed at 793 K, which is a temperature much lower than 873 K. This has benefits for PbTe as a thermoelectric material that is sensitive to sublimation at higher temperatures.

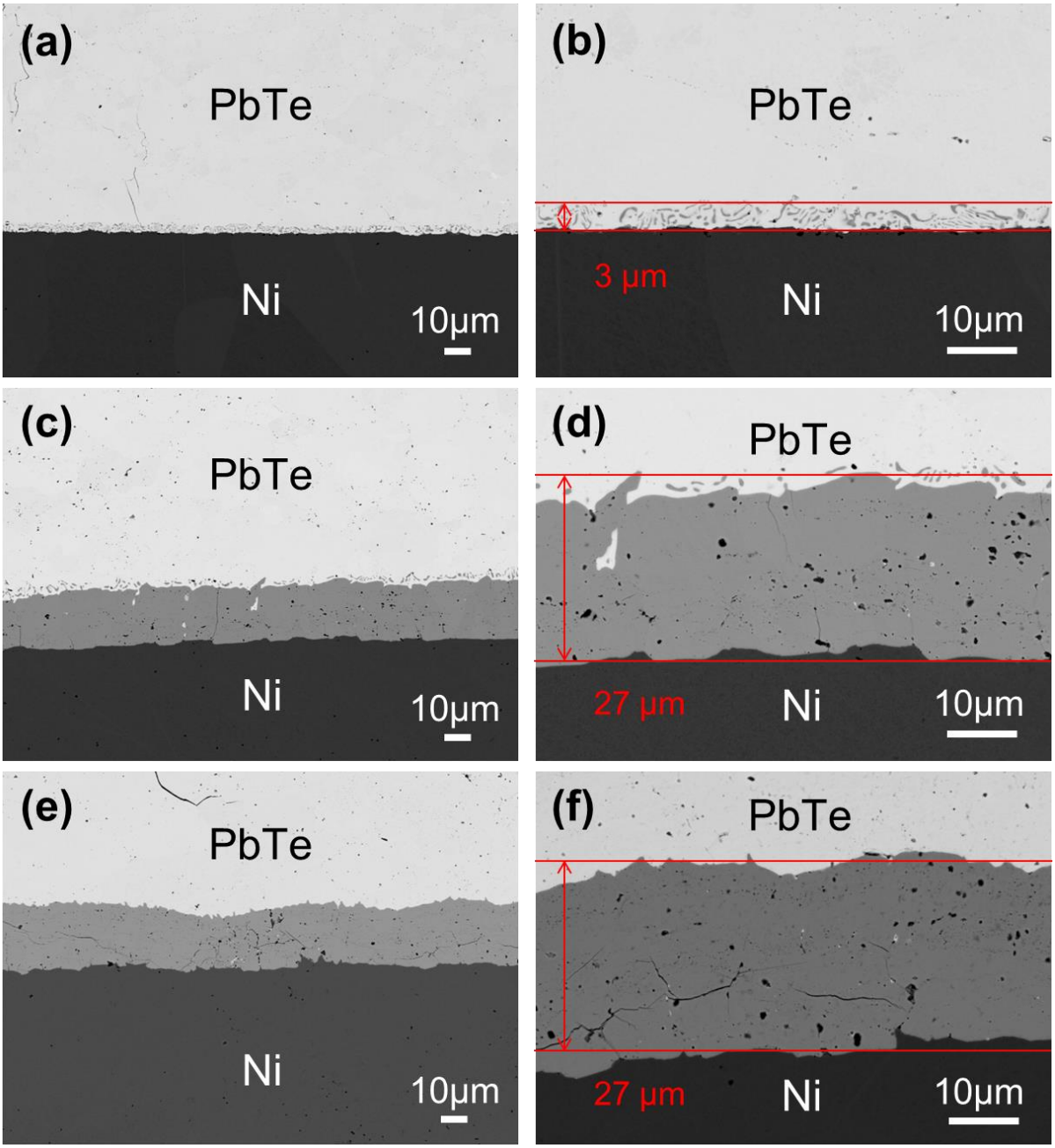

Figure 6. SEM micrographs of the bonding area between PbTe and Ni after sintering under 40 MPa pressure for 10 minutes at temperatures of (a) and (b) 723 K; (c) and (d) 793 K; (e) and (f) 873 K.

The obtained bond in this study satisfies expectations by forming a homogeneous diffusion barrier in the contact area between the thermoelectric material and the nickel electrode by a one-step sintering process. The composition of the generated interphase is consistent with Ni_3Te_2 as the only intermetallic formed during the reaction. An earlier study [11] on the one-step bonding of Ni to *n*-type PbTe by rapid hot pressing found defects at the junction with the nickel electrode, which increased in number with the sintering time, allowing PbTe to diffuse and react inside the cracks. The main reported composition is $Ni_{3\pm x}Te_2$ (38.6 - 41.0 at.% Te), and a ternary phase of $Ni_5Pb_2Te_3$ is observed together with it via a eutectic reaction at the Ni/PbTe interface at 923 K. The continuous diffusion of

elements into the defects in Ni electrode, where they can react at the device operating temperature, was introduced as the major limitation of this sort of fabricated interface.

We have formed a defect-free, fully reacted interface between Ni and PbTe. The nickel electrode is free of defects, allowing homogeneous diffusion of the interlayer into the PbTe. The intermetallic formed is also the binary Ni_3Te_2 compound, and there is no evidence of a ternary phase. We believe that our interphase could better prevent further reaction between the Ni electrode and the thermoelectric material.

Aging test

The highest performance of PbTe materials is obtained at 700 – 850 K [30], promoting the fabrication of thermoelectric generators designed to work at a similar hot side temperature. These conditions can be applied for an extended period of time, and therefore, long-term thermal stability of the interface is essential for future thermoelectric module performance. Sublimation is the main degradation mechanism for thermoelectric generators. If sublimation of materials at the hot side junction is significant over time, it could cause mechanical failure of the contact between the interphase and the thermoelectric material. The standard cross-sectional reduction due to sublimation is around 5-10% over a 10 year period. The sublimation rate of PbTe at 530°C is about 2×10^{-7} g/cm^{-2} h and 7×10^{-7} g/cm^{-2} h for 5% and 10% reduction, respectively [38]. In order to examine the thermal stability of the fabricated Ni/PbTe joints, an aging test at 803 K was conducted under vacuum. Figure 7 shows an optical microscope image after the joint was exposed to high-temperature conditions for 360 hours. The image proves that there is clear degradation of PbTe. The increase in porosity and cracks within the thermoelectric material exemplifies the effects of the sublimation mechanism at 823 K. With long-term usage, this could be detrimental to power performance or lead to mechanical failure between bonded layers. Despite the obvious damage to the sample after the test, we still observed a well-defined and continuous interphase.

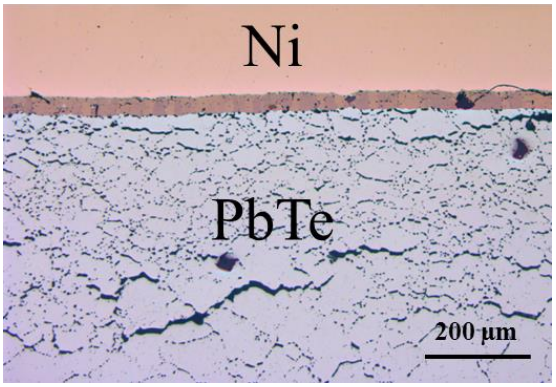

Figure 7. Optical microscope image after the sample was encapsulated in a quartz tube under vacuum and aged for 360 hours at 823 K.

EBSD analysis and energy dispersive X-ray spectroscopy (EDS) were also performed simultaneously on the thermally aged sample, which was prepared in the same way as the as-sintered sample. The analysis was performed to investigate any changes in the crystallographic structure of the interphase after the long-term thermal aging test. Figure 8 presents the band contrast (Figure 8(a)) and phase distribution (Figure 8(b)) maps. The indexing of the EBSD map clearly delineates three phases, which are presented in light red (Ni), blue (Ni_3Te_2), and yellow (PbTe). This identifies the β_2 $Ni_{3\pm x}Te_2$ monoclinic phase as the sole composition of the interphase. Therefore, the chemical stability of the Ni_3Te_2 compound is confirmed by the absence of any evidence of its reactivity with respect to Ni and PbTe. The presence of twins is also noticeable at the grains of the Ni_3Te_2 phase. Twins are shown in dark red and have the same 82.5°/<110> angle-axis relationship as in the as-sintered sample. With respect to the Ni_3Te_2 diffusion layer, cracks and porosity have increased compared to the as-sintered sample. These are represented in the EBSD map (Figure 8(b)) as unindexed white areas. Moreover, a slight separation between the Ni (light red) and Ni_3Te_2 (blue) phases is observed. This effect could have been caused by the cutting of the cross-section to perform the microscopic analysis. This is plausible due to the weakening of the interface bond that was caused by the larger number of pores in the diffusion barrier layer. Otherwise, we suggest that differences in the coefficients of thermal expansion (CTE) were responsible for the cracking. No information is available in the literature on the CTE of Ni_3Te_2 phase, so it is impossible to draw a conclusion on this matter. EDS maps of the Ni, interphase, and PbTe interfaces for the aged sample are presented in Figure 8(c), (d), and (e). The micrographs show a distinct interphase containing Ni and Te between the Ni electrode and the PbTe thermoelectric material. The elemental distribution of the three layers resembles that in the as-sintered sample, with an interphase thickness of roughly 30 μm. It appears that the wide Ni_3Te_2 diffusion barrier layer prevented diffusion of Ni into the PbTe phase. Two possible reaction products are reported between Ni_3Te_2 and PbTe [39]: Ni_2PbTe_4 [39] and Ni_3PbTe_3 [36]. There is no thermodynamic data available for these phases, however, and we observed no new phases that were formed during the aging test, as is evident from the EDS analysis shown in Figure 8(c-e). Blocking any continuous reaction with PbTe is essential for maintaining bonding performance. The chemical composition and thickness of the barrier layer of Ni_3Te_2 remain constant after the aging test, proving the effectiveness of the present bonding method between Ni electrode and *n*-type PbTe.

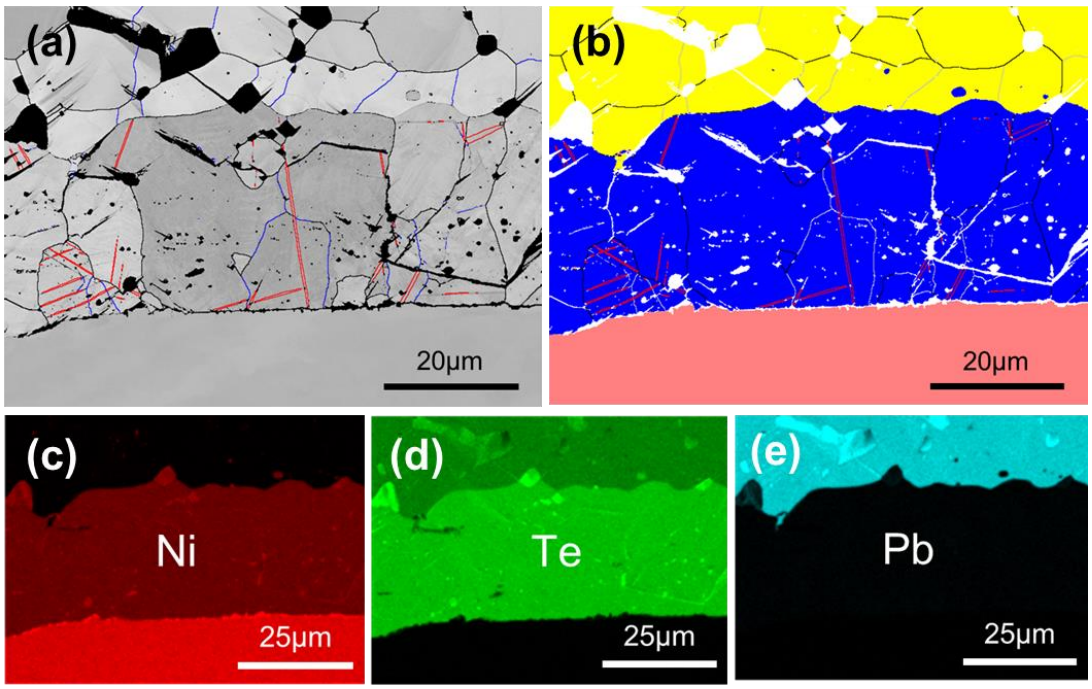

Figure 8. (a) EBSD band contrast map, (b) EBSD phase distribution map. EDS mapping of PbTe/Ni aged thermally at 823 K for 360 hours: (c) Ni elemental mapping, (d) Te elemental mapping, (e) Pb elemental mapping.

Conclusions

Nickel plate was successfully bonded to *n*-type PbTe by one-step sintering using SPS. The β_2 phase $Ni_{3\pm x}Te_2$ was identified as the sole compound formed at the Ni/PbTe interface. A uniform interphase layer of Ni_3Te_2 with a continuous thickness of ~30 μm was achieved at 793 K within 10 minutes. No defects were observed on the Ni electrode, allowing the reaction to occur in the contact area between the nickel and the lead telluride. Testing after thermal aging at 823 K for 360 hours showed the chemical stability of the fabricated interphase, with no significant increase in the thickness. This confirms that no further reaction occurs between PbTe and Ni at the aging temperature. Nevertheless, degradation of PbTe was observed after aging, suggesting that lower application temperatures should be selected for generators fabricated from PbTe. The interphase achieved herein is a suitable diffusion barrier, and one-step sintering of PbTe powder to Ni electrode is a promising technique for fabrication of thermoelectric generators from PbTe.

Acknowledgments

This work was supported by an Australian Research Council (ARC) Linkage Project (LP120200289), an ARC Discovery Early Career Award (DE130100310), and the AutoCRC (Project Agreement 1-203). The authors would like to thank the Electron Microscopy Centre (EMC) at the University of

Wollongong for offering access to microscopes and sample preparation equipment.

References

[1] A.D. LaLonde, Y. Pei, G.J. Snyder, Reevaluation of $PbTe_{1-x}I_x$ as high performance *n*-type thermoelectric material, Energy & Environmental Science. 4 (2011) 2090-2096.

[2] C.M. Jaworski, J.P. Heremans, Thermoelectric transport properties of the *n*-type impurity Al in PbTe, Physical Review B. 85 (2012) 033204.

[3] S. Aminorroaya Yamini, H. Wang, D. Ginting, D.R. Mitchell, S.X. Dou, G.J. Snyder, Thermoelectric Performance of *n*-Type $(PbTe)_{0.75}(PbS)_{0.15}(PbSe)_{0.1}$ Composites, ACS Applied Materials & Interfaces. 6 (2014) 11476-11483.

[4] K. Biswas, J. He, I.D. Blum, C.-I. Wu, T.P. Hogan, D.N. Seidman, et al., High-performance bulk thermoelectrics with all-scale hierarchical architectures, Nature. 489 (2012) 414-418.

[5] Y. Pei, A. LaLonde, S. Iwanaga, G.J. Snyder, High thermoelectric figure of merit in heavy hole dominated PbTe, Energy & Environmental Science. 4 (2011) 2085-2089.

[6] S.A. Yamini, D.R. Mitchell, Z.M. Gibbs, R. Santos, V. Patterson, S. Li, et al., Heterogeneous Distribution of Sodium for High Thermoelectric Performance of *p*-type Multiphase Lead-Chalcogenides, Advanced Energy Materials. 5 (2015).

[7] L.E. Bell, Cooling, Heating, Generating Power, and Recovering Waste Heat with Thermoelectric Systems, Science. 321 (2008) 1457-1461.

[8] G.J. Snyder, E.S. Toberer, Complex thermoelectric materials, Nature Materials. 7 (2008) 105-114.

[9] X.F. Zheng, Y.Y. Yan, K. Simpson, A potential candidate for the sustainable and reliable domestic energy generation–Thermoelectric cogeneration system, Applied Thermal Engineering. 53 (2013) 305-311.

[10] H.J. Goldsmid, The Thermoelectric and Related Effects, In: R. Hull, J. R.M. Osgood, J. Parisi, H. Warlimont, editors, Introduction to Thermoelectricity. Berlin, Heidelberg: Springer; (2010) 1-6.

[11] H. Xia, C.L. Chen, F. Drymiotis, A. Wu, Y.Y. Chen, G.J. Snyder, Interfacial Reaction Between Nb Foil and n-Type PbTe Thermoelectric Materials During Thermoelectric Contact Fabrication, Journal of Electronic Materials. 43 (2014) 4064-4069.

[12] T. Chuang, H. Lin, C. Chuang, W. Yeh, J. Hwang, H. Chu, Solid Liquid Interdiffusion Bonding of (Pb, Sn) Te Thermoelectric Modules with Cu Electrodes Using a Thin-Film Sn Interlayer, Journal of Electronic Materials. 43 (2014) 4610-4618.

[13] V.K. Valery, Reliability Issues in Electrical Contacts, In: M.O. Thurston, editor, Electrical Contacts. Boca Raton: CRC Press; (2006) 205-259.

[14] Mohamed S. El-Genk, H.H. Saber, Modeling and Optimization of Segmented Thermoelectric Generators for Terrestrial and Space Applications, In: D.M. Rowe, editor, Thermoelectrics Handbook. Taylor & Francis Group, LLC; (2006).

[15] K. Arai, M. Matsubara, Y. Sawada, T. Sakamoto, T. Kineri, Y. Kogo, et al., Improvement of Electrical Contact Between TE Material and Ni Electrode Interfaces by Application of a Buffer Layer, Journal of Electronic Materials. 41 (2012) 1771-1777.

[16] J.E. Ni, E.D. Case, R.D. Schmidt, C.-I. Wu, T.P. Hogan, R.M. Trejo, et al., The thermal expansion coefficient as a key design parameter for thermoelectric materials and its relationship to processing-dependent bloating, Journal of Materials Science. 48 (2013) 6233-6244.

[17] V. Ravi, S. Firdosy, T. Caillat, E. Brandon, K. Van Der Walde, L. Maricic, et al., Thermal Expansion Studies of Selected High-Temperature Thermoelectric Materials, Journal of Electronic Materials. 38 (2009) 1433-1442.

[18] Y. Hikage, S. Masutani, T. Sato, S. Yoneda, Y. Ohno, Y. Isoda, et al., Thermal expansion properties of thermoelectric generating device component. Proceedings of 26th International Conference on Thermoelectrics (ICT'07): IEEE; (2007) 331-335.

[19] M. Weinstein, A.I. Mlavsky, Bonding of Lead Telluride to Pure Iron Electrodes, Review of Scientific Instruments. 33 (1962) 1119-1120.

[20] C. Long, Y. Yan, J. Zhang, B. Ren, Z. Wang, New integration technology for PbTe element. Proceedings of 25th International Conference on Thermoelectrics (ICT'06): IEEE; (2006) 386-389.

[21] M. Orihashi, N. Yasutoshi, L. Chen, Y. Kang, A. Moro, T. Hirai, Ni/*n*-PbTe and Ni/*p*-$Pb_{0.5}Sn_{0.5}Te$ joining by plasma activated sintering. Proceedings of 17th International Conference on Thermoelectrics (ICT 98): IEEE; (1998) 543-546.

[22] C. Yang, H. Lai, J. Hwang, T. Chuang, Diffusion Soldering of Pb-Doped GeTe Thermoelectric Modules with Cu Electrodes Using a Thin-Film Sn Interlayer, Journal of Electronic Materials. 42 (2013) 359-365.

[23] Y. Lan, D. Wang, G. Chen, Z. Ren, Diffusion of nickel and tin in *p*-type $(Bi, Sb)_2Te_3$ and *n*-type $Bi_2(Te, Se)_3$ thermoelectric materials, Applied Physics Letters. 92 (2008) 101910-101910.

[24] J. García-Cañadas, A. Powell, A. Kaltzoglou, P. Vaqueiro, G. Min, Fabrication and Evaluation of a Skutterudite-Based Thermoelectric Module for High-Temperature Applications, Journal of Electronic Materials. 42 (2013) 1369-1374.

[25] J. de Boor, C. Gloanec, H. Kolb, R. Sottong, P. Ziolkowski, E. Müller, Fabrication and characterization of nickel contacts for magnesium silicide based thermoelectric generators, Journal of Alloys and Compounds. 632 (2015) 348-353.

[26] R.K. Bordia, H. Camacho-Montes, Sintering: Fundamentals and Practice, In: N.P. Bansal, A.R. Boccaccini, editors, Ceramics and Composites Processing Methods. John Wiley & Sons, Inc.; (2012) 1-42.

[27] J. Fan, L. Chen, S. Bai, X. Shi, Joining of Mo to $CoSb_3$ by spark plasma sintering by inserting a Ti interlayer, Materials Letters. 58 (2004) 3876-3878.

[28] T. Sui, J.F. Li, S.Z. Jin, Joining $CoSb_3$ to Metal Surface of FGM Electrode for Thermoelectric Modules by SPS, Key Engineering Materials. 368 (2008) 1858-1861.

[29] D.M. Rowe, CRC Handbook of Thermoelectrics: Macro to Nano, Boca Ratcon: CRC Taylor & Francis. (2006).

[30] A.D. LaLonde, Y. Pei, H. Wang, G.J. Snyder, Lead telluride alloy thermoelectrics, Materials Today. 14 (2011) 526-532.

[31] R.G.J. Ball, S. Dickinson, E.H.P. Cordfunke, R.J.M. Konings, J. Drowart, S. Smoes, Thermochemical data acquisition-Part II. Commission of the European Communities; (1992).

[32] L.D. Gulay, I.D. Olekseyuk, Crystal structures of the compounds Ni_3Te_2, $Ni_{3-\delta}Te_2$ (δ=0.12) and $Ni_{1.29}Te$, Journal of Alloys and Compounds. 376 (2004) 131-138.

[33] Y. Zhang, X. Ke, C. Chen, J. Yang, P.R.C. Kent, Thermodynamic properties of PbTe, PbSe, and PbS: First-principles study, Physical Review B. 80 (2009) 024304.

[34] Y.K. Rao, Stoichiometry and thermodynamics of metallurgical processes: Cambridge University Press (CUP) Archive. (1985).

[35] H. Xia, F. Drymiotis, C.L. Chen, A. Wu, G.J. Snyder, Bonding and interfacial reaction between Ni foil and *n*-type PbTe thermoelectric materials for thermoelectric module applications, Journal of Materials Science. 49 (2014) 1716-1723.

[36] C.I. Abilov, Projection of the liquidus surface of the system Pb-Ni-Te, Zhurnal Neorganicheskoi Khimii. 34 (1989) 1004-8.

[37] S.I. Kim, K.H. Lee, H.A. Mun, H.S. Kim, S.W. Hwang, J.W. Roh, et al., Dense dislocation arrays embedded in grain boundaries for high-performance bulk thermoelectrics, Science. 348 (2015) 109-114.

[38] J. Yang, T. Caillat, Thermoelectric Materials for Space and Automotive Power Generation, MRS Bulletin. 31 (2006) 224-229.

[39] C.I. Abilov, Z.A. Iskenderzade, Interaction of PbTe with Ni_3Te_2, Inorganic Materials. 25 (1989) 213-215.